THE JOURNAL OF PHYSICAL CHEMISTRY B

ARTICLE

pubs.acs.org/JPCB

Conformational Variability of Organophosphorus Hydrolase upon Soman and Paraoxon Binding

Diego E. B. Gomes,[†] Roberto D. Lins,[‡] Pedro G. Pascutti,[†] Chenghong Lei,[§] and Thereza A. Soares*[,‡]

[†]Instituto de Biofísica Carlos Chagas Filho, Universidade Federal do Rio de Janeiro, Rio de Janeiro, RJ 21949-900, Brazil

[‡]Departamento de Química Fundamental, Universidade Federal de Pernambuco, Recife, PE 50740-540, Brazil

[§]Pacific Northwest National Laboratory, P.O. Box 999, MSIN K7-90, Richland, Washington 99352, United States

ABSTRACT: The bacterial enzyme organophosphorus hydrolase (OPH) exhibits both catalytic and substrate promiscuity. It hydrolyzes bonds in a variety of phosphotriester (P−O), phosphonothioate (P−S), phosphofluoridate (P−F), and phosphonocyanate (F−CN) compounds. However, its catalytic efficiency varies markedly for different substrates, limiting the broad-range application of OPH as catalyst in the bioremediation of pesticides and chemical war agents. In the present study, pK_a calculations and multiple explicit-solvent molecular dynamics (MD) simulations were performed to characterize and contrast the structural dynamics of OPH bound to two substrates hydrolyzed with very distinct catalytic efficiencies: the nerve agent soman (*O*-pinacolylmethylphosphonofluoridate) and the pesticide paraoxon (diethyl *p*-nitrophenyl phosphate). pK_a calculations for the substrate-bound and unbound enzyme showed a significant pK_a shift from standard values (ΔpK_a = ±3 units) for residues His254 and Arg275. MD simulations of protonated His254 revealed a dynamic hydrogen bond network connecting the catalytic residue Asp301 via His254 to Asp232, Asp233, Arg275, and Asp235, and is consistent with a previously postulated proton relay mechanism to ferry protons away from the active site with substrates that do not require activation of the leaving group. Hydrogen bonds between Asp301 and His254 were persistent in the OPH−paraoxon complex but not in the OPH−soman one, suggesting a potential role for such interaction in the more efficient hydrolysis of paraoxon over soman by OPH. These results are in line with previous mutational studies of residue His254, which led to an increase of the catalytic efficiency of OPH over soman yet decreased its efficiency for paraoxon. In addition, comparative analysis of the molecular trajectories for OPH bound to soman and paraoxon suggests that binding of the latter facilitates the conformational transition of OPH from the open to the closed substate promoting a tighter binding of paraoxon.

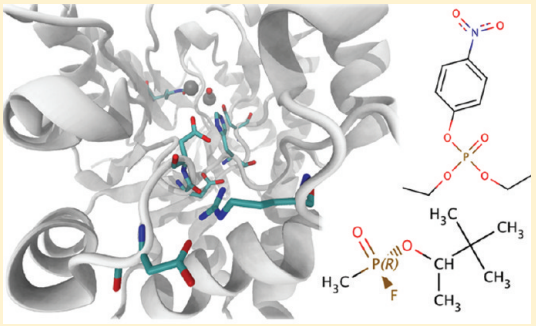

INTRODUCTION

Organophosphorus (OP) compounds are extremely toxic substances used exclusively as insecticides and chemical warfare agents (e.g., sarin, soman, and XV).[1] The acute toxicity of OP results primarily from the inactivation of the enzyme acetylcholine esterase through the irreversible phosphorylation of an active site serine, which leads to interruption of acetylcholine breakdown in nervous synapses and red blood cell membranes.[2−4] Other known direct targets of OP intoxication include the muscarinic and nicotinic acetylcholine receptors.[5,6] Phosphotriesterases are a group of enzymes that can degrade OP compounds and have a great potential for use in bioremediation and detection technologies through their confinement within nanoscale structures.[7−10] The enzyme organophosphorus hydrolase (OPH; EC 3.1.8.1) from the soil bacteria *Brevundimonas diminuta* (previously *Pseudomonas diminuta*) is the best-characterized phosphotriesterase.[11−16] OPH hydrolyzes bonds in a variety of phosphotriester (P−O), phosphonothioate (P−S), phosphofluoridate (P−F), and phosphonocyanate (F−CN) compounds with high catalytic efficiency and broad substrate specificity.[12,13,17−21] Typical turnover rates for the best OPH substrate, paraoxon, exceed 10^4 s^{-1}, while the corresponding values for k_{cat}/K_M approach the diffusion limit of 10^7 M^{-1} s^{-1}.[17,21,22] In contrast, the chemical hydrolysis of paraoxon by KOH occurs with a second-order rate constant of only 10^{-2} M^{-1} s^{-1}.[22] Another major feature of OPH is its stereoselectivity for the hydrolysis of chiral organophosphate triesters, since major chemical warfare agents are racemic mixtures with substantial differences in toxicity of the individual enantiomers. However, the catalytic activity of OPH toward these racemic nerve agents is not as efficient as toward paraoxon. For instance, the R_PR_C enantiomer of soman is hydrolyzed by OPH with k_{cat} of 48 s^{-1} and k_{cat}/K_M in the order of 10^4 M^{-1} s^{-1}. Such enantiomer is soman's configuration most efficiently catalyzed by the wild-type OPH.[20]

Crystallographic structures have shown that OPH is a homodimeric $(\alpha/\beta)_8$-barrel protein containing one active site per monomer.[11] Each active site is composed of two divalent metal ions bridged by a μ-hydroxo ion and by a carbamylated lysine

Received: September 12, 2011
Revised: November 6, 2011
Published: November 17, 2011

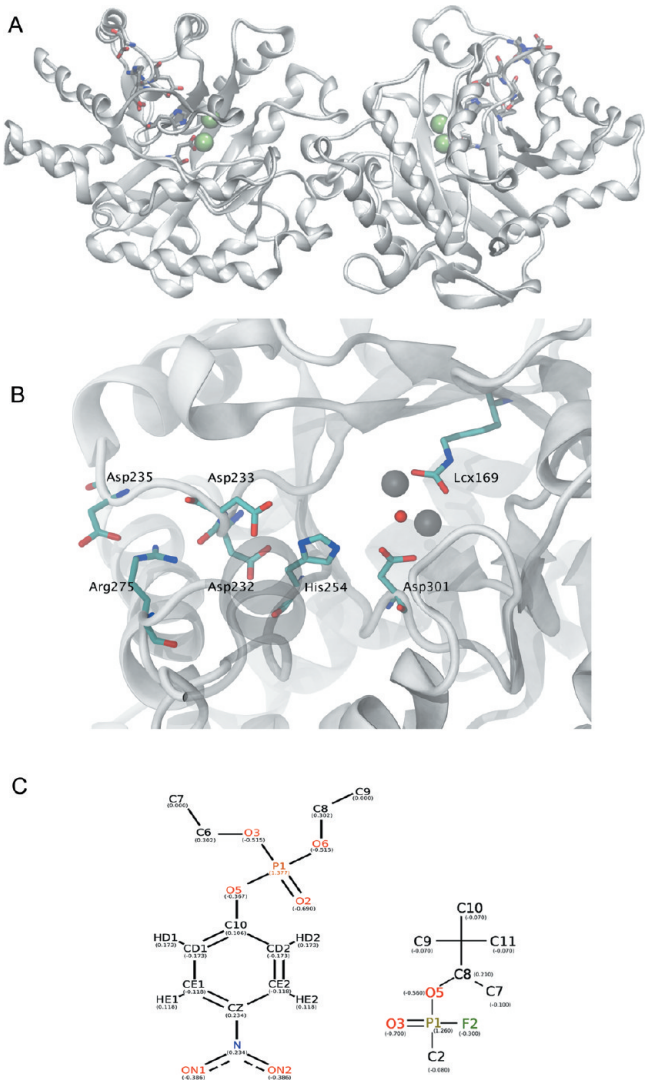

Figure 1. (A) Crystallographic structure of homodimeric organophosphorus hydrolase (OPH). (B) Detail of the active-site region and residues of the putative proton shuttle (one subunit). Zn^{2+} cations (green/gray spheres) are bridged by the μ-hydroxo ion (red sphere) and by the carbamylated lysine residue (Lcx169). (C) Chemical structure of paraoxon and soman with the atomic charges used in the simulations.

residue (Figure 1). Zn^{2+} is the apparent native metal, although substantial activity is observed after substitution of the binuclear metal center by Co^{2+}, Cd^{2+}, Mn^{2+}, or Ni^{2+}.[11] Two metal ions per active site are required for full catalytic activity, and kinetic constants k_{cat} and k_{cat}/K_M are dependent upon the identity of the specific metal cations within the active site. The hydrolysis of organophosphate triesters by OPH has been shown to occur through an inversion of stereochemical configuration at the phosphorus center in a S_N2 mechanism without formation of any covalent substrate−enzyme intermediate.[23] A reaction mechanism has been postulated where the organophosphate substrate binds to the active site by displacement of a water molecule coordinating the β-metal cation.[24] Subsequently, the metal oxygen interaction polarizes the phosphoryl oxygen bond and makes the phosphorus center more electrophilic for the nucleophilic attack of the μ-hydroxo ion.[25] The proton from the resulting hydroxyl group is then transferred to Asp301 and shuttled away with the assistance of His254 and Asp233. This last step has been suggested to enhance significantly the reactivity of the metal-bridging nucleophile since mutation of either His254 or Asp233 resulted in a decrease in the kinetic constants for paraoxon.[24]

Although a S_N2 mechanism has been recognized for the hydrolysis of organophosphate triesters by OPH, several modifications to the postulated mechanism have been proposed from recent experimental and computational studies.[26−28] An important point of debate concerns the identity of the nucleophile. Jackson and co-workers[27] have argued that the metal bridging μ-hydroxo does not act as the initiating nucleophile, but instead acts as a general base for a nucleophilic water molecule coordinated to the α-metal cation. Computational studies using QM/MM and high-level QM calculations indicate that His254 acts as a base to activate and deprotonate the hydroxide nucleophile.[26,28] Another aspect that has just begun to be addressed is the role of substrate binding in the turnover rates of OPH which is limited by either conformational change or diffusion.[17] Recently, Jackson and co-workers have shown that OPH mutants exhibit "closed" and "open" conformational substates which are either optimally preorganized for paraoxon hydrolysis but preclude its access to/from the active site or allow easy substate access to the active site but are poorly organized for hydrolysis.[29] The transition between these unique conformational substates is governed by conformational changes of a specific region (loop 7) of the protein, whose propensity to adopt different conformations is directly associated with the different catalytic efficiencies exhibited by the respective substates.

In the present study, we have performed a systematic investigation of the conformational dynamics of the free and substrate-bound OPH taking into consideration the protonation states of residues predicted to have large pK_a shifts, namely His254 and Arg275. The chosen substrates are the pesticide paraoxon (diethyl *p*-nitrophenyl phosphate) and the nerve agent soman (*O*-pinacolylmethylphosphonofluoridate) which are hydrolyzed by the wild-type OPH at rather distinct catalytic efficiency rates (10^7 and 10^5 M^{-1} s^{-1}, respectively).[20,30] By exploring possible combinations of the most probable protonation states of OPH residues, it has been found that, in addition to residues His254 and Asp301, residues Asp232, Asp235, and Arg275 take part in a hydrogen-bond network that may serve as the proton-shuffling pathway proposed by Aubert and co-workers.[24] The persistence of these interactions is modulated by the presence and identity of the substrate. Likewise, the transition between the open and closed OPH substates is observed exclusively in the presence of the substrate paraoxon.

COMPUTATIONAL METHODOLOGY

High-resolution crystallographic structures of OPH from *Brevundimonas diminuta* were used as initial coordinates in the MD simulations (PDB ID 1EZ2 and 1HZY).[11,31] The cocrystallized substrate analogue diisopropylmethyl phosphonate was replaced by the paraoxon or the R_PR_C−soman enantiomer. The R_PR_C enantiomer of soman is the configuration most efficiently catalyzed by the wild-type OPH.[20] The replacement of diisopropylmethyl phosphonate by soman was achieved by replacing one of the isopropyl groups by a fluorine atom and the other by the pinacolyl group. For paraoxon, each isopropyl group of the diisopropylmethyl phosphonate was replaced by an ethyl group and the *p*-nitrophenyl group was bonded to the phosphate group. Missing atoms in the crystallographic structures were verified and

Table 1. Molecular Systems[a]

	protonation state				atom number		
simulations	^{257}His	Arg275	substrate	time (ns)	solute	solvent	ions
HdRp	neutral	protonated	none	10		83310	0
HdRd	neutral	neutral	none	10		84000	$2Na^+$
HpRp	protonated	protonated	none	50		83295	$2Cl^-$
HpRd	protonated	neutral	none	50		83994	$2Cl^-$, $2Na^+$
HpRp-Par	protonated	protonated	paraoxon	50		77688	$2Cl^-$
HpRd-Par	protonated	neutral	paraoxon	50		77688	0
HpRp-Som	protonated	protonated	soman	50		73862	$2Cl^-$
HpXRd-Som	protonated	neutral	soman	50		74303	0

[a] Simulations vary for the protonation states of residues His254 and Arg275, presence or absence of substrates, type of substrates, and simulation time. The metal bridging group was a hydroxyl ion for all simulations.

added if necessary via the WHAT IF web server.[32] Atom additions were necessary only to the terminal residues. Protonation states were assigned accordingly to pK_a calculations with the program propKa version 2.0.[33] The homodimers were represented identically concerning the protonation state of residues as well as the presence or absence of the substrate. All simulations were carried out using the GROMOS force field force parameter set 53A6.[34,35] A description of the simulated systems is presented in Table 1. The active site of OPH contains two zinc ions bridged by a hydroxide anion and a carbamylated lysine. The zinc and hydroxide ions were treated as a nonbonded model with a formal charge of +3*e*. The carbamylated lysine had a formal charge of −1*e*. Charges for the hydroxide ion and carbamylated lysine were assigned via a restrained hyperbolic fit of the electrostatic potential (RESP)[36] on the nuclei positions of each atom after geometry optimizations at the HF-6-31G* level using the NWCHEM software[37] as described in ref 38. This same approach was used to calculate atomic charges for substrates soman and paraoxon (Figure 1C).

The systems were placed in a rectangular box (average dimensions of $12.8 \times 9.0 \times 8.0$ nm^3), treated for periodic boundary conditions, and solvated with explicit SPC model water molecules.[39] The systems were neutralized with Na^+ counterions where necessary. Simulations were carried out in the NPT ensemble, and a time step of 1 fs was used to integrate the equations of motion based on the Leap-Frog algorithm.[40] The temperature of the solute and solvent were separately coupled to the velocity rescale thermostat at 298.15 K with a relaxation time of 0.1 ps. The pressure was maintained as 1 atm by isotropic coordinate scaling with a relaxation time of 1 ps. The bond lengths and angles were constrained by using the P-LINCS algorithm,[41] and the geometry of the water molecules was constrained using the SETTLE algorithm.[42] A twin-range cutoff of 1.0 and 1.2 nm was used for vdW interactions, and long-range electrostatic interactions were treated by the particle mesh Ewald method.[43] The systems were initially minimized through 20 000 iterations of the steepest descent algorithm. Solvent molecules were relaxed during 500 ps of simulation at 298.15 K with positional restraints applied to the heavy atoms of the protein. The full system was equilibrated for 10 ns followed by the production phase of 50 ns. Configurations of the system were recorded as trajectory files at every 1.0 ps. The software package GROMACS v.4.04 (double precision) and implemented algorithms were used for all simulations and property analyses.[44] Protein structures were visualized with the software VMD 1.86.[45] Metadynamics calculations[46,47] were performed with Plumed plugin[48] in GROMACS v.4.5.1.[44] A one-dimensional collective variable was defined as the distance between the residues of OPH active site and the center of mass of each bound substrate. The 50 ns structure of the complex OPH—paraoxon was used as starting point for metadynamics calculations. Simulations were carried out in explicit solvent for 5 ns with a 1 fs time step where 5000 Gian hills were added. A hill is a potential describing the opposite of a potential well and corresponds to the region surrounding a local maximum.[46,47] The height of the metadynamics hills was 0.35 kJ/mol and width of 0.05 nm.

Table 2. Residues of the Active-Site Region with Large pK_a Shifts

	pK_a (units)		
PDB id	His254	Arg275	resolution (Å)
OPH_{wt} (2OB3)	9.6	9.2	1.04
OPH_{wt} (1EZ2)	10.0	9.4	1.90
OPH_{wt} (1HZY)	9.7	9.2	1.30
OPH_{D233A} (1HZY)	3.4	9.4	1.30
OPH_{D233N} (1HZY)	−0.7	9.2	1.30
pK_a model compound[a]	6.5	12.5	N/A

[a] From reference (Li, Robertson, and Jensen, 2005).

RESULTS

Protonation States of Residues His254 and Arg275. pK_a values were calculated for all ionizable residues of OPH using several high-resolution X-ray structures of the enzyme and the program propKa version 2.0 (Table 2).[33] The calculations were performed for the wild-type and two mutant forms of the enzyme, namely D233A and D233N. The catalytic activities of Asp233 mutants were previously characterized for substrate paraoxon, and the residue was proposed to participate in the shuttling of protons from the active site.[24] Two residues in the active site displayed pK_a values significantly shifted from their standard values. The pK_a of His254 was shifted from 6.5 units to values in the range of 9.6−10.0 units whereas Arg275 exhibits pK_a values shifted from 12.5 units to 9.2−9.4 units. OPH displays a maximal activity in the pH range of 9−9.5 units for the hydrolysis of paraoxon,[49−51] which corresponds approximately to the estimated

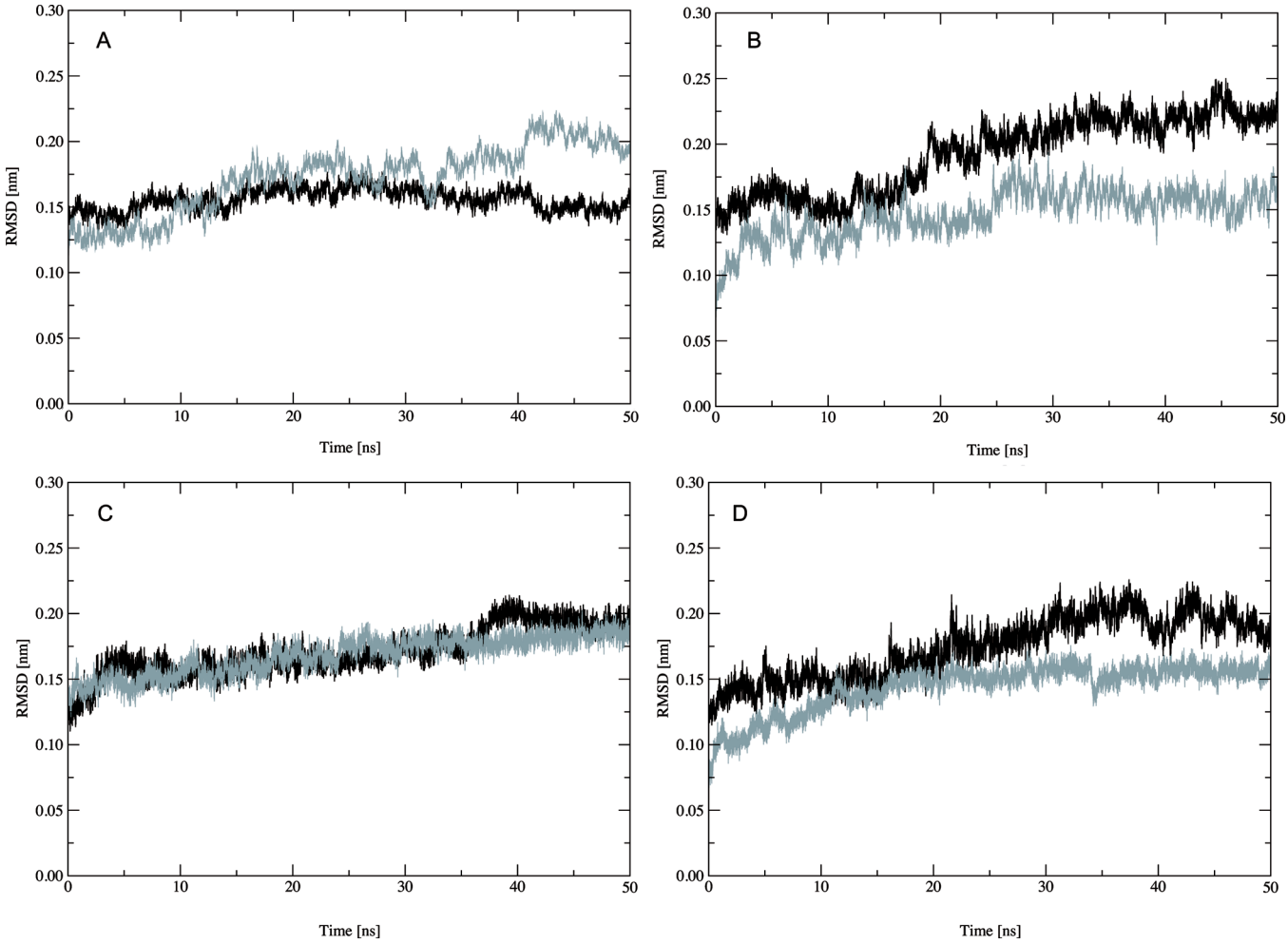

Figure 2. Root-mean-square deviation (rmsd) of backbone atoms of OPH from the X-ray structure (1HYZ) as function of the protonation states of residues His254 and Arg275 for the substrate-bound and unbound enzyme. (A) Protonated (black) and neutral (gray) His254 in the unbound OPH. Protonated (black) and neutral (gray) Arg275 in the unbound OPH (B), in paraoxon-bound OPH (C) and in soman-bound OPH (D). Arg275 is neutral in A whereas His254 is protonated in B−D. Rotational and translational fitting of pairs of structures was applied using all backbone atoms. Values are averaged for the two monomers.

pK_a of the two residues. It can be inferred from the crystallographic data that both residues are involved in interactions to catalytic residues: His254 makes hydrogen bonds to Asp301 and Asp233 whereas Arg275 is spatially close to Asp233, near the end of a small cleft leading outward from the active site. Furthermore, random directed evolution studies have supported the importance of residue His254 in the enhancement of OPH hydrolysis rates of several toxic compounds, including V-agents and the G-agents.[52−54]

The effect of the D233A and D233N mutations on the pK_a of surrounding residues is restricted to His254 (Table 2). Both mutations lead to a large decrease of the pK_a of His254 but have no effect on the pK_a of Arg275. Residue Asp301 exhibits invariably negative pK_a values which indicate that this residue is deprotonated even at very low pH (data not shown). The insensitivity of the protonation state of Asp301 to nearby mutations can be explained by its proximity to positively charged Zn^{2+} cations, making its pK_a less responsive to the suppression of comparatively smaller charges, e.g., mutations D233A and D233N. Because the accuracy of FDPB methods is highly correlated to the quality of the structural data,[55,56] it should be noticed that the X-ray structures of OPH used for the pK_a calculations were solved at very high resolution, near 1.0 Å[11] and exhibited very low *B* factors, particularly the active-site region (on average below 20 Å^2). It was previously shown via MD simulations,[38] and later corroborated via crystallographic studies of the highly homologous (>90% similarity) OPH from *Agrobacterium radiobacter*,[29] that OPH conformational changes are mostly limited to the side chains of loop residues in the entrance of the active site. In the active site, most residues exhibit a rather rigid geometry due to the strong electrostatic interactions to the divalent cations. These experimental and computational data support the assumption that the X-ray structure of OPH is representative of one predominant conformation, further corroborated by recent findings from Jackson and co-workers.[29] On this account, it is reasonable to assume that the protonation states assigned to such conformation are the predominant ones at a given pH. These protonation states were treated via independent simulations of the respective states (see Table 1).

Conformational Dynamics of the OPH upon Substrate Binding. The structural dynamics of the enzyme active site was investigated as a function of distinct ionization states of residues

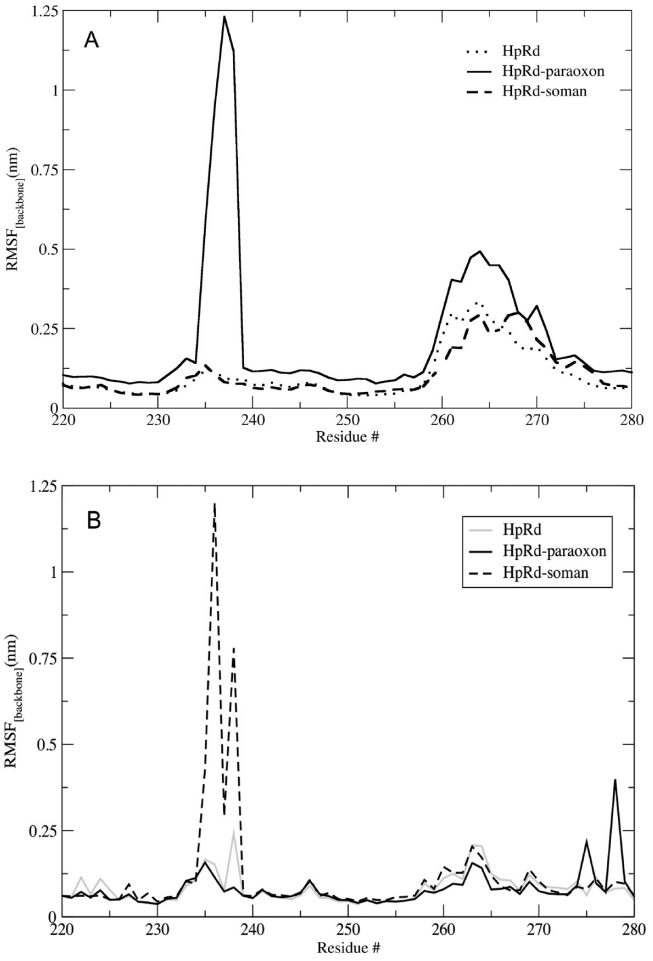

Figure 3. Atom-positional root-mean-square fluctuations (RMSF) of backbone atoms averaged per residue (aa 220 to 280) for the substrate free (HpRd) and substrate-bound OPH (HpRd−paraoxon and HpRd−soman). Values are averaged for the two OPH monomers and (A) over 50 ns of simulations or (B) over the final 2 ns of simulations.

His254 and Arg275, and the presence of either a very efficient substrate (paraoxon) or a very inefficient one (soman).[20,30] The simulated systems are presented in Table 1. Atom-positional root-mean-square deviations were calculated for backbone atoms in the MD trajectories with respect to their positions in the X-ray structure (1HYZ) (Figure 2). Average rms deviations for the simulated systems are between 0.14 and 0.19 nm, reaching a first plateau around 10 ns. In the neutral state, His254 moves away from the metal center, disrupting the hydrogen bond interactions to Asp301 and Asp233 observed in the crystallographic structure. This event occurs within 1 ns of simulation, in the presence or absence of the substrate, and after 1 ns long equilibration using distance positional restraints between these residues (Figure 2). Therefore, only the protonated state of His254 generated a conformational ensemble consistent with the X-ray structure, and the simulation HdRp was discontinued after 10 ns (Figure 2). In the absence of the substrates, there is a small but steady increase of the rms deviations for system HpRp compared to system HpRd. This increase (up to 0.7 Å) of the backbone atom-positional rms deviation for HpRp over HpRd reflects solely the presence/absence of one single proton. The effect of the protonation of Arg275 on the backbone rms deviations is less evident in the presence of the substrates, particularly if compared the same substrate, indicating a decrease of conformational flexibility upon substrate binding to OPH. The subsequent analysis described here will revolve around the protonated states of His254 and Arg275, either in the absence (HpRp) or presence of substrates paraoxon (HpRd-Par) and soman (HpRd-Som).

It has been previously shown that OPH conformational changes are mostly limited to loop residues in the entrance of the active site.[27,29,38,57] Atom-positional root-mean-square fluctuations (RMSF) were calculated for backbone atoms in the HpRd, HpRd-Par, and HpRd-Som trajectories with respect to the initial conformation (Figure 3A) as well as the MD-final conformation (Figure 3B) aiming at the comparison of the regions whose dynamics differs among these systems. Two regions comprising residues 234−239 and 258−275 exhibit rather distinct atom-positional fluctuation amplitudes for HpRd-Par with respect to the HpRd and HpRd-Som simulations. Residues 258−275 have been designated as loop 7 by Jackson and coworkers,[29] and residues 234−239, which correspond to a preceding helix/loop motif will therefore be designated as loop 6 (Figure 4). The large atomic fluctuations observed in the paraoxon-bound ensemble are due to the displacement of these residues toward the active site, nearly closing its cleft (Figure 4). A considerably larger displacement is associated to loop 6 in presence of paraoxon, but it is not affected by the presence of soman (Figure 3A). No discernible rearrangement is observed for loop 6 either in the soman-bound or substrate-free enzyme conformations (Figures 3 and 4). These findings are further confirmed by comparison of the RMSF calculated over the entire 50 ns and the last 2 ns of simulations for HpRd-paraoxon, HpRd-Som, and HpRd (Figure 3A,B). The RMSF analysis shows that the large atomic fluctuations in the HpRd−paraoxon simulations over the 50 ns of simulations decrease significantly during the final 2 ns, i.e., after the loops have closed over the active-site cleft. The opposite behavior is observed for HpRd−soman, which shows low RMSF values over the period of 50 ns, and then an increase of atomic fluctuations during the last 2 ns of simulations. However, such RMSF increase over the last 2 ns of simulations does not lead to the displacement of loops 6 and 7 over the active site. Most likely, longer simulations will be necessary to sample the complete displacement of the region onto the active-site cleft process for HpRd−soman. It should also be noticed that the conformational rearrangement of loops 6 and 7 does not alter its secondary structure content (data not shown). These results indicate that, upon paraoxon binding, OPH undergoes a structural transition involving loops 6 and 7 located at the entrance of the active site. Such transition leads to a "closed" conformational substate, which allows for tighter fitting of the paraoxon substrate into the enzyme's active site.

Time-dependent solvent-accessible surface area (SASA) has also been calculated for the ensemble of structures from the simulations of the substrate-bound enzymes (HpRd-Par and HpRd-Som) in the absence of the respective substrates (Figure 5). Only residues lining the active-site cavity were used for the SASA calculations in order to estimate its dimensions in the substrate-bound and free enzymes along the simulated time. These residues are F132, R254, Y257, and L271. After a period of 50 ns, the active site of the paraoxon-bound enzyme is nearly 75 $Å^2$ smaller than that of the soman-bound OPH, consistent with the closure of active-site entry by loops 6 and 7 in the presence of the fast substrate (Figure 5). The event leading to the loop displacement toward the active site takes place very rapidly, at around 30 ns.

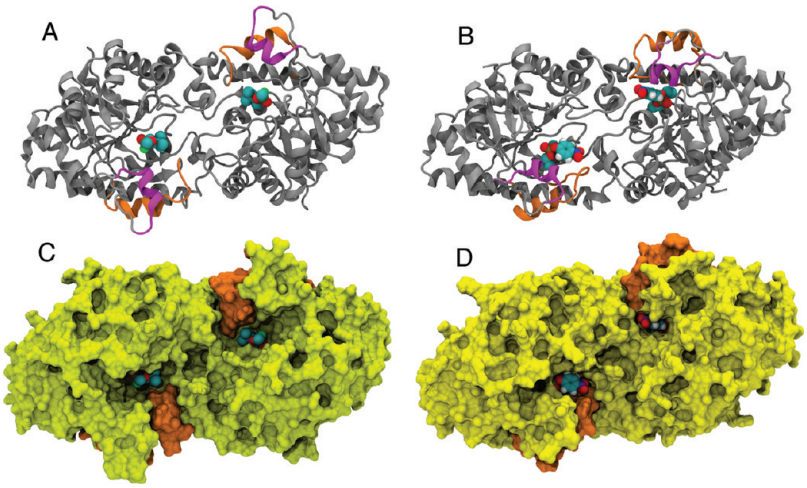

Figure 4. Conformational substates of soman- and paraoxon-bound OPH after 50 ns simulations. Cartoon representation of the enzyme bound to the substrates soman (A) and paraoxon (B) represented by the CPK model (carbon in cyan, oxygen in red, nitrogen in blue, and hydrogen atoms in white). Regions corresponding to loop 7 and associated helix are shown in orange while loop 6 and its helix are shown in magenta. (C,D) Molecular surface representation of the same conformations of soman- and paraoxon-bound OPH, respectively. The region corresponding to loop 7 and its helix is colored in magenta.

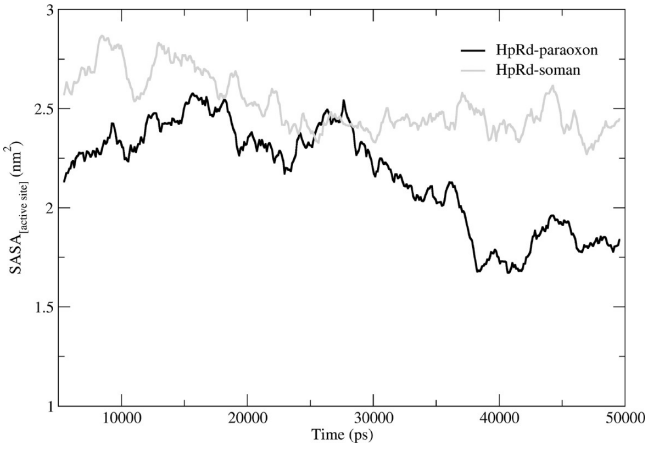

Figure 5. Solvent-accessible surface area (SASA) of the OPH active site bound to soman and paraoxon as a function of simulation time. The active-site cavity is entirely circumscribed by residues F132, R254, Y257, and L271, which were used to calculate SASA. Values are averaged over the active site of the two monomers.

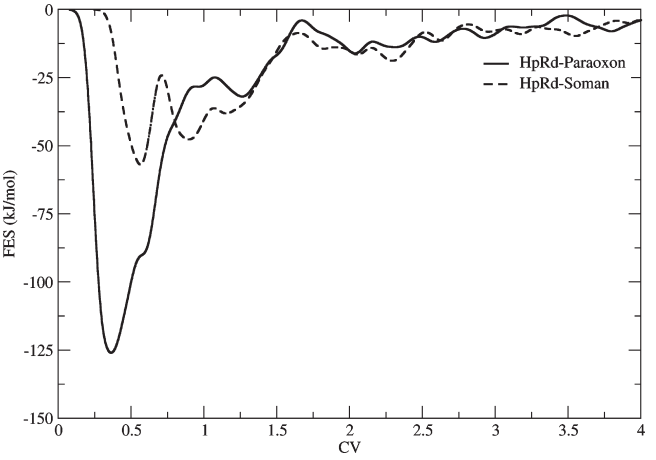

Figure 6. Dissociation free energy profiles for soman and paraoxon from their respective OPH conformational substates after 50 ns simulations.

Such event is not observed upon soman binding to OPH for the time scale simulated here. The relative energy barrier for the dissociation of paraoxon and soman from the active site of the enzyme has been estimated by the means of metadynamics calculations using a one-dimensional collective variable defined as the distance between the active-site residues and the substrates (Figure 6). The relative dissociation free energy profile shows that pulling paraoxon from the active site would cost an additional −69 kJ/mol (−16.5 kcal/mol) over soman. This energy cost is associated with the conformational rearrangement of loops 6 and 7 required for the binding/unbind of paraoxon onto the active site of OPH. Conversely, soman can be easily released from the active site since it binds/unbinds without any significant conformational rearrangement at the simulated time scale.

Hydrogen-Bond Occupancies. Analyses of hydrogen-bond occupancies Q were performed for residues His254 and Arg275 in six simulations (Table 3). In these simulations, His254 can make hydrogen bonds to residues Asp232, Asp301, and Asp253. The interaction between residues His254 and Asp233 observed in crystalline conditions appears to occur more transiently in solution. In solution conditions, Asp232 replaces Asp233 as the most persistent hydrogen-bond partner of protonated His254. In the absence of the substrate, protonated His254 interacts with all three aspartate residues, whereas deprotonated His254 interacts predominantly to Asp253. In the presence of the substrate, hydrogen bonds between His254 and Asp232 and/or Asp301 have significantly higher occupancies than that between His254 and Asp253 (Table 3). The hydrogen bond between His254 and Asp301 has the highest occupancy upon paraoxon binding to OPH, being present during one-fourth to half of the simulated time for this complex. This is in contrast to the same interaction in the complex OPH−soman, which has the lowest occupancy among all the simulated systems where His254 is protonated (Table 3). Residue Arg275 forms hydrogen bonds to residues Asp232, Asp233, and Asp235 (Table 3), with the prevalence of each one of these interactions being correlated with the protonation

Table 3. Hydrogen Bond Occupancies Q for Unbound and Substrate-Bound OPH with Different Protonation States of His254 and Arg275[a]

		occupancy Q (%)					
		His254			Arg275		
simulations	protonation State	Asp232	Asp301	Asp253	Asp232	Asp233	Asp235
HdRd	$Arg275_{neutral}$	≤9.0	≤0.6	73.4	92.8	0.0	≤3.7
HdRp	$Arg275_{protonated}$	≤9.0	≤0.6	71.6	49.5	6.9	56.4
HpRd	$Arg275_{neutral}$	60.1	17.5	34.8	94.2	1.2	11.6
HpRp	$Arg275_{protonated}$	88.5	14.5	16.8	13.1	20.1	36.3
HpRd-Par	$Arg275_{neutral}$	100.0	26.0	≤0.5	100.0	0.1	≤6.4
HpXRp-Par	$Arg275_{protonated}$	94.5	47.2	≤0.5	21.1	13.2	26.5
HpRd-Som	$Arg275_{neutral}$	77.3	≤3.8	22.4	52.1	0.0	24.4
HpRp-Som	$Arg275_{protonated}$	100.0	≤3.8	≤3.3	≤1.6	29.1	35.5

[a] Hydrogen bonds between side-chain donor−acceptor atoms (histidine $N\delta_1$, $N\varepsilon_2$; aspartic acid $O\varepsilon_1$, $O\varepsilon_2$; and arginine $N\varepsilon$, $N\eta_1$, $N\eta_2$).

state of residue Arg275. Protonated Arg275 favors interactions with the backbone carbonyl and the side-chain carboxyl groups of residue Asp232 whereas deprotonated Arg275 interacts more often with the side-chain carboxyl group of residues Asp233 and Asp235. The protonation state of Arg275 has no apparent effect on the hydrogen-bond interactions made by His254, with the exception of the interaction between His254 and Asp253 in the system HpRd-Som (Table 3). Yet, the remaining interactions between His254 in this system follow the same pattern as in system HpRp-Som. It is interesting to note that, in the X-ray crystal structure of the H254G/H257W/L303T mutant OPH, the substitution of His254 with a glycine yields a cavity where a third metal can bind, being coordinated by Asp253.[53] These results indicate that ^{253}Asp can adopt various conformations without major changes in the overall conformation of the enzyme.

Wild-type OPH exhibits very distinct catalytic efficiency values for the hydrolysis of paraoxon and soman (10^7 and 10^5 M^{-1} s^{-1}, respectively).[20,30] The catalytic role of Asp301 is well established in the hydrolysis of both susbtrates. It has also been previously shown that mutations of His254 decrease the catalytic efficiency of OPH over paraoxon, with rate constants of 1−3 orders of magnitude smaller than those for the wild-type enzyme.[24] Single mutations of His254 also decrease the catalytic efficiency of OPH over different enantiomers of soman, though to a smaller extent compared to paraoxon.[13,20,53] It can be inferred from the present simulations that the hydrogen bond between Asp301 and His254 occurs with a higher probability upon paraoxon binding to OPH (26%−47%) compared to soman (<3.8%) and taking as reference the free enzyme (14.5%−17.5%) (Table 3). Although a direct relationship between the presence of Asp301/His254 hydrogen-bond and substrate hydrolysis cannot be presently established, these findings suggest that such interaction may be of relevance to the more efficient hydrolysis of paraoxon over soman by the wild-type OPH. At the level of the Michaelis complex, this hydrogen bond helps to position Asp301 with respect to the metal-bridging hydroxide ion to bring about the reaction, and as discussed thereafter, could offer a a potential pathway for proton relay after catalysis.

DISCUSSION

A Potential Pathway for Proton Relay in the Hydrolysis Reaction Catalyzed by OPH. The hydrolysis of organophosphate triesters by OPH follows a S_N2 reaction.[23] The postulated mechanism for this reaction proposes that the hydroxide ion bridging the metal ions promotes a nucleophilic attack on the phosphorus center of the substrate. The bond to the leaving group phenol is broken, and the proton from the nucleophilic hydroxide is transferred to Asp301 and from it to His254 and other residues in a proton relay mechanism. Lately, several modifications to this mechanism[24] have been proposed based on recent experimental and computational studies.[26−28] In one variation of this mechanism, the μ-hydroxo is proposed to act as a general base activating a water molecule terminally coordinated to the α-metal.[27] The proton from the water molecule is shuttled from the active site via the μ-hydroxo bridge and the proton relay system. In another variation of the original mechanism,[26] the metal-bridging hydroxide ion also initiates the nucleophilic attack on the phosphorus center of the substrate, but in contrast to the original mechanism, His254 is protonated and loses its proton to the solvent as the leaving group departs from the active site. In the next step of the proposed reaction, His254 acts as a base to activate and deprotonate the water nucleophile, though the authors point out that the role as a specific or general base may also be undertaken by another water molecule.[24,26]

The results presented here suggest that the protein environment causes the pK_a of His254 to shift from 6.5 units to 9.6−10.0 units (Table 2). Considering that OPH displays maximal activity in the pH range of 9−9.5 units,[49−51] His254 is likely to be protonated upon binding of the substrate. Furthermore, the MD simulations show that only the protonated state of His254 yields a conformational ensemble consistent with the X-ray structures, which have been solved at pH 9.0.[11,31] If His254 is represented in its deprotonated state, it moves away from the metal center and disrupts the hydrogen bond to Asp301. These results are consistent with the structure of the Michaelis complex in the catalytic mechanism proposed by Wong and Gao[26] using a QM/MM approach based on AM1 semiempirical potentials. On the basis of the good agreement between the simulated structural properties, the experimental data, and the higher-level QM calculations, we have investigated a potential pathway for the proton relay mechanism proposed Raushel and co-workers.[24] These authors have suggested the existence of a proton relay from Asp301 to His254 to Asp233 used to ferry protons away from the active site during reactions with substrates that do not require activation of the leaving group phenol such as paraoxon.[24] The conformational dynamics of active-site residues in the complex OPH−paraoxon

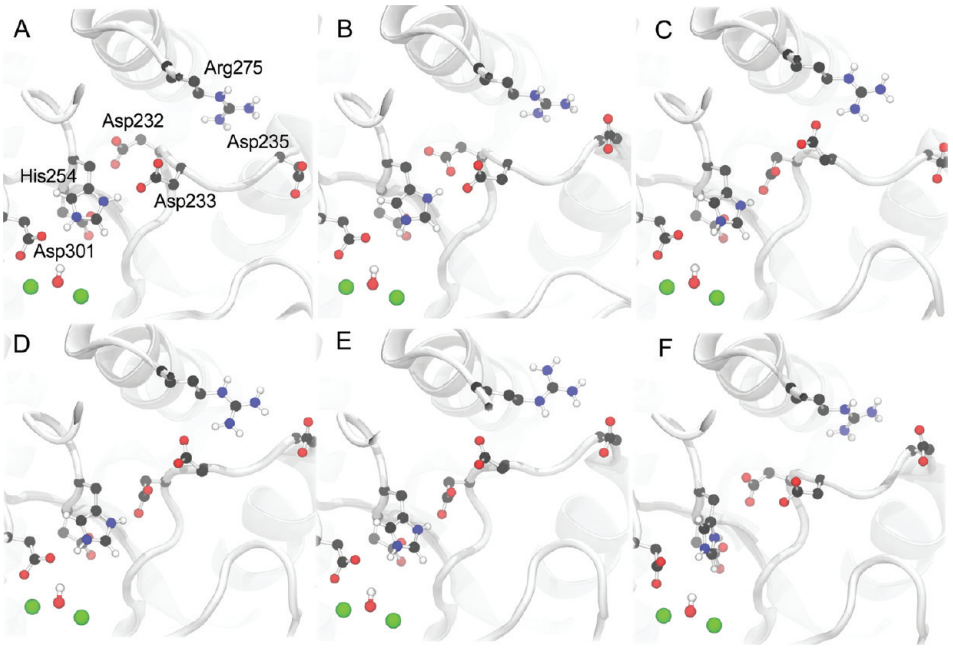

Figure 7. Proposed proton pathway after the hydrolysis of paraoxon by OPH. (A) Active-site conformation (frame collected at 1.3 ns) which is analogous to the X-ray structure; (B) His254 interacts simultaneously with Asp233 and Asp232 (frame collected at ca. 1.1 ns); (C) Asp233 makes a hydrogen bond with Arg275 whereas His254 now interacts only with Asp232 (frame collected at ca. 1.8 ns); (D) Arg275 forms a hydrogen bond with Asp235 (frame collected at ca. 1.9 ns); (E) Arg275 flips (frame collected at ca. 4.4 ns); and (F) His254 (frame collected at ca. 1.5 ns) interacts with Asp253 in the absence of the substrate.

exhibit a pattern of interactions suggestive of a potential pathway for the proposed proton relay (Figure 7).[24] In the MD simulations of these systems (HpRp-par, HpRd-par), His254 (protonated) makes a persistent hydrogen bond to Asp301 and a less stable one to Asp233 (Figure 7A). The latter interaction is replaced around 2 ns by a hydrogen bond to Asp232 (Figure 7B) whereas Asp233 undergoes a conformational change (Figure 7C), interacting simultaneously to Asp232 and Arg275 (Figure 7D). The residue Arg275 can flip over itself, interacting either to Asp233 or to Asp235 (Figure 7E,F). Residues Arg275 and Asp235 are located in the solvent-exposed entrance to the active site where the proton can be transferred to the bulk solvent.

Conformational Substates and Substrate Binding to OPH. Proteins explore a range of conformations via internal motions on a wide range of time scales. These time scales include localized motion such as bond vibrations, rotations of side chains, and fluctuations within a group of few atoms on the picosecond—nanosecond time scale as well as large-scale collective fluctuations involving subdomains transitions on the nanosecond—millisecond time scale and up.[58−60] Recently, it has become apparent that conformational fluctuations from the concerted motions of many atoms can lead the unbound states (substates) of enzymes into conformations very similar to the bound states, molding them to form complexes with specific ligands.[61−68] Such fluctuations are not random despite the inherent flexibility of the unbound state of a protein and occur preferentially in a way that prepares the protein to bind to its ligands.[58,61] Hence, enzymatic efficiency (fast rates for formation of the Michaelis complex, the chemical reaction, and product release) could be made possible via fluctuations between different conformational substates with unique configurations and catalytic properties.[62,63,65,69]

The hydrolysis of paraoxon by OPH takes place with turnover rates of 10^4 s^{-1} and k_{cat}/K_M values that approach the diffusion limit of 10^7 M^{-1} s^{-1}.[17,21,22] These rates are phosphoric acid by a physical barrier,[17,70] i.e., either substrate diffusion or conformational change. Recent kinetics and structural characterization of OPH mutants have shown that the enzyme exhibits "open" and "closed" conformational substates.[29] The closed substate is optimally preorganized for paraoxon hydrolysis but access to/from the active site is obstructed by structural rearrangements of loop 7. The open conformational substate allows easy substrate access to the active site but is poorly organized for hydrolysis. Further, changes to the reaction rate due to mutations mostly result from changes in the activation entropy and not in the activation energy for the transition between conformational substates. Hence, the "open" and "closed" substates of OPH coexist in equilibrium in the resting enzyme whereby conformational transitions between them is used to tune the conformational landscape to maximize the rate of substrate and product diffusion.[29] The newly proposed[29] schematic for OPH catalytic cycle is

$$E_{closed} \overset{fast}{\rightleftharpoons} E_{open} + S \underset{k_2}{\overset{k_1}{\rightleftharpoons}} E_{open}S \overset{fast}{\rightleftharpoons} E_{closed}S$$

$$\xrightarrow{k_3} E_{closed}P \overset{fast}{\rightleftharpoons} E_{open}P \xrightarrow{k_5} E_{open} + P$$

The present simulations of OPH show that indeed there is a structural transition involving loop 7 as well as loop 6 (the latter not previously observed in the crystallographic studies) which blocks the access to the active site. The event is observed for paraoxon-bound but not for free and soman-bound OPH conformational ensembles (Figure 3A). Comparison of the final conformations for paraoxon- and soman-bound OPH shows a snug fit of the former substrate into the active site of the enzyme whereas the latter substrate fits rather loosely into the cleft (Figure 4, c and d). The energy difference to pull the two substrates away

from the active site indicates that paraoxon interacts more favorably with the enzyme than does soman (ca. −69 kJ/mol) (Figure 6). Therefore, paraoxon-bound OPH transitions between $E_{open}S$ to $E_{closed}S$ substates whereas soman-bound OPH remains in the $E_{open}S$ substate for the simulated time scale. The transition between $E_{open}S$ to $E_{closed}S$ substates upon paraoxon-binding is fast, being complete in less than 50 ns. Based on the condition that fast conformational change in OPH allows rapid fluctuation between conformational substates preorganized for different steps in turnover,[29] the slower substate transition exhibited by soman-bound OPH would be expected to decrease its catalytic efficiency toward this substrate.

CONCLUSION

Several long-scale molecular dynamics (MD) simulations were performed for OPH unbound and bound to two substrates hydrolyzed with very distinct catlytic efficiencies: the nerve agent soman (*O*-pinacolylmethylphosphonofluoridate) and the pesticide paraoxon (diethyl *p*-nitrophenyl phosphate). Different protonation states of the residues His254 and Arg275 were also taken into account in the simulations. The choice of residues was based on their predicted large pK_a shifts from standard values ($\sim\Delta pK_a = \pm 3$ units) and on their potential role in the hydrolysis reaction catalyzed by OPH. In the X-ray structures these residues are well positioned to form hydrogen bonds to several aspartic acid residues near the divalent metals, including Asp233 and Asp301. It has been found that (i) there is a decrease of conformational flexibility of OPH upon substrate binding; (ii) only the protonated state of His254 yielded a conformational ensemble consistent with the X-ray structures; (iii) the calculated pK_a for His254 is in the range of 9.6−10.0 units offering support to a predominantly protonated state for this residue during the enzymatic catalysis and in agreement with the results of Wong and Gao;[26] (iv) a dynamical hydrogen-bond network involving residues Asp301, His254, Asp232, Asp233, Arg275, and Asp235 may function as a pathway to shuttle protons away from the active site as previously proposed by Raushel and co-workers;[24] and (v) the transition between the open and closed OPH substates has been observed only for paraoxon-bound OPH within the 50 ns time scale, suggesting that such transition occurs at a faster rate for paraxon-bound than soman-bound OPH. Fast conformational change in OPH leads to rapid fluctuation between conformational substates preorganized for different steps in turnover.[29] Therefore, it would be expected that the slower substate transition exhibited by soman-bound OPH would translate into decreased catalytic efficiency toward this substrate.

AUTHOR INFORMATION

Corresponding Author

*E-mail: thereza.soares@ufpe.br.

ACKNOWLEDGMENT

This work was supported by the Brazilian National Council for Research and Development (CNPq), FACEPE, INCT/INAMI, nBioNet, and the National Institute of General Medical Sciences (grant no. R01GM080987). Computational resources were provided by the Environmental Molecular Sciences Laboratory at Pacific Northwest National Laboratory. Pacific Northwest National Laboratory is operated for DOE by Battelle.

REFERENCES

(1) Gunderson, C. H.; Lehmann, C. R.; Sidell, F. R.; Jabbari, B. *Neurology* **1992**, *43*, 946.
(2) Brown, M. A.; Brix, K. A. *J. Appl. Toxicol.* **1998**, *6*, 393.
(3) Holstege, C. P.; Kirk, M.; Sidell, F. R. *Critical Care Clinics* **1997**, *13*, 923.
(4) Sogrob-Sanchez, M. A.; Vilanova-Gisbert, E.; Carrera-Gonzalez, V. *Rev. Neurociencia* **2004**, *39*, 739.
(5) Bakry, N. M.; el-Rashidy, A. H.; Eldefrawi, A. T.; Eldefrawi, M. E. *J. Biochem. Toxicol.* **1988**, *3*, 235.
(6) Mileson, B. E.; Chambers, J. E.; Chen, W. L.; Dettbarn, W.; Ehrich, M.; Eldefrawi, A. T.; Gaylor, D. W.; Hamernik, K.; Hodgson, E.; Karczmar, A. G.; et al. *Toxicol. Sci.* **1998**, *41*, 8.
(7) Gomes, D. E.; Lins, R. D.; Pascutti, P. G.; Straatsma, T. P.; Soares, T. A. *Lect. Notes Comput. Sci.: Adv. Bioinf. Comput. Biol.* **2008**, *5167*, 68.
(8) Lei, C.; Shin, Y.; Liu, J.; Ackerman, E. J. *J. Am. Chem. Soc.* **2002**, *124*, 11242.
(9) Lei, C.; Soares, T. A.; Shin, Y.; Liu, J.; Ackerman, E. J. *Nanotechnology* **2008**, *19*, 125102.
(10) Lei, C. H.; Valenta, M. M.; Saripalli, K. P.; Ackerman, E. J. *J. Environ. Qual.* **2007**, *36*, 233.
(11) Benning, M. M.; Shim, H.; Raushel, F. M.; Holden, H. M. *Biochemistry* **2001**, *40*, 2712.
(12) Chen-Goodspeed, M.; Sogorb, M. A.; Wu, F. Y.; Hong, S. B.; Raushel, F. M. *Biochemistry* **2001**, *40*, 1325.
(13) Chen-Goodspeed, M.; Sogorb, M. A.; Wu, F. Y.; Raushel, F. M. *Biochemistry* **2001**, *40*, 1332.
(14) Raushel, F. M. *Curr. Opin. Chem. Microbiol.* **2002**, *5*, 288.
(15) Raushel, F. M.; Holden, H. M. *Adv. Enzymol.* **2000**, *74*, 51.
(16) Wu, F. Y.; Li, W. S.; Chen-Goodspeed, M.; Sogorb, M. A.; Raushel, F. M. *J. Am. Chem. Soc.* **2001**, *122*, 10206.
(17) Caldwell, S. R.; Newcomb, J. R.; Schlechtand, K. A.; Raushel, F. M. *Biochemistry* **1991**, *30*, 7438.
(18) Gopal, S.; Rastogi, V.; Ashman, W.; Mulbry, W. *Biochem. Biophys. Res. Commun.* **2000**, *279*, 516.
(19) Li, W. A.; Aubert, S. D.; Raushel, F. M. *J. Am. Chem. Soc.* **2003**, *125*, 7526.
(20) Li, W. A.; Lum, K. T.; Chen-Goodspeed, M.; Sogorb, M. A.; Raushel, F. M. *Bioorg. Med. Chem.* **2001**, *9*, 2083.
(21) Omburo, G. A.; Kuo, J. M.; Mullins, L. S.; Raushel, F. M. *J. Biol. Chem.* **1992**, *267*, 13278.
(22) Dumas, D. P.; Wild, J. R.; Raushel, F. M. *Experientia* **1990**, *46*, 729.
(23) Lewis, V. E.; Donarski, W. J.; Wild, J. R.; Raushel, F. M. *Biochemistry* **2001**, *27*, 1591.
(24) Aubert, S. D.; Li, Y. C.; Raushel, F. M. *Biochemistry* **2004**, *43*, 5707.
(25) Samples, C. R.; Raushel, F. M.; DeRose, V. J. *Biochemistry* **2007**, *46*, 3435.
(26) Wong, K. Y.; Gao, J. *Biochemistry* **2007**, *46*, 13352.
(27) Jackson, C. J.; Foo, J. L.; Kim, H. K.; Carr, P. D.; Liu, J. W.; Salem, G.; Ollis, D. L. *J. Mol. Biol.* **2008**, *375*, 1189.
(28) Zhang, X.; Wu, R.; Song, L.; Lin, Y.; Lin, M.; Cao, Z.; Wu, W.; Mo, Y. *J. Comput. Chem.* **2009**.
(29) Jackson, C. J.; Foo, J. L.; Tokuriki, N.; Afriat, L.; Carr, P. D.; Kim, H. K.; Schenk, G.; Tawfik, D. S.; Ollis, D. L. *Proc. Natl. Acad. Sci. U. S.A.* **2009**, *106*, 21631.
(30) Omburo, G. A.; Mullins, L. S.; Raushel, F. M. *Biochemistry* **1993**, *32*, 9148.
(31) Benning, M. M.; Hong, S. B.; Raushel, F. M.; Holden, H. M. *J. Biol. Chem.* **2000**, *275*, 30556.
(32) Rodriguez, R.; Chinea, G.; Lopez, N.; Pons, T.; Vriend, G. *Bioinformatics* **1998**, *14*, 523.
(33) Bas, D.; Rogers, D. M.; Jensen, J. H. *Proteins: Struct. Funct. Bioinf.* **2008**, *73*, 765.
(34) Oostenbrink, C.; Soares, T. A.; van der Vegt, N. F. A.; van Gunsteren, W. F. *Eur. Biophys. J. Biophys.* **2005**, *34*, 273.

(35) Soares, T. A.; Daura, X.; Oostenbrink, C.; Smith, L. J.; van Gunsteren, W. F. *J. Biomol. NMR* **2004**, *30*, 407.
(36) Cornell, W. D.; Cieplak, P.; Bayly, C. I.; Kollman, P. A. *J. Am. Chem. Soc.* **1993**, *115*, 9620.
(37) Straatsma, T. P.; Aprà, E.; Windus, T. L.; Bylaska, E. J.; de Jong, W.; Hirata, S.; Valiev, M.; Hackler, M.; Pollack, L.; Harrison, R. et al. NWChem, A Computational Chemistry Package for Parallel Computers, Version 4.6; Pacific Northwest National Laboratory: Richland, WA 99352−0999, 2004.
(38) Soares, T. A.; Osman, M.; Straatsma, T. P. *J. Chem. Theory Comput.* **2007**, *3*, 1569.
(39) Berendsen, H. J. C.; Postma, J. P. M.; van Gunsteren, W. F.; Hermans, J. Interaction models for water in relation to protein hydration. In *Intermolecular Forces*; Pullman, B., Ed.; Reidel: Dordrecht, The Netherlands, 1981; p 331.
(40) van Gunsteren, W. F.; Berendsen, H. J. C. *Mol. Simul.* **1988**, *1*, 173.
(41) Hess, B.; Bekker, H.; Berendsen, H. J. C.; Fraaije, J. G. E. M. *J. Comput. Chem.* **1997**, *18*, 1463.
(42) Miyamoto, S.; Kollman, P. A. *J. Comput. Chem.* **1992**, *13*, 952.
(43) Essmann, U.; Perera, L.; Berkowitz, M. L.; Darden, T.; Lee, H.; Pedersen, L. G. *J. Chem. Phys.* **1995**, *103*, 8577.
(44) Hess, B.; Kutzner, C.; van der Spoel, D.; Lindahl, E. *J. Chem. Theory Comput.* **2008**, *4*, 435.
(45) Humphrey, W.; Dalke, A.; Schulten, K. *J. Mol. Graphics* **1996**, *14*, 33.
(46) Barducci, A.; Bussi, G.; Parrinello, M. *Phys. Rev. Lett.* **2008**, *100*, 020603.
(47) Laio, A.; Parrinello, M. *Proc. Natl. Acad. Sci. U.S.A.* **2002**, *99*, 12562.
(48) Bonomi, M.; Branduardi, D.; Bussi, G.; Camilloni, C.; Provasi, D.; Raiteri, P.; Donadio, D.; Marinelli, F.; Pietrucci, F.; Broglia, R. A. *Comput. Phys. Commun.* **2009**, *180*, 1961.
(49) Rochu, D.; Viguie, N.; Renault, F.; Crouzier, D.; Froment, M. T.; Masson, P. *Biochem. J.* **2004**, *380*, 627.
(50) Raushel, F. M.; Holden, H. M. *Adv. Enzymol. Relat. Areas Mol. Biol.* **2000**, *74*, 51.
(51) Donarski, W. J.; Dumas, D. P.; Heitmeyer, D. P.; Lewis, V. E.; Raushel, F. M. *Biochemistry* **1989**, *28*, 4650.
(52) diSioudi, B.; Grimsley, J. K.; Lai, K.; Wild, J. R. *Biochemistry* **1999**, *38*, 2866.
(53) Hill, C. M.; Li, W. S.; Thoden, J. B.; Holden, H. M.; Raushel, F. M. *J. Am. Chem. Soc.* **2003**, *125*, 8990.
(54) Reeves, T. E.; Wales, M. E.; Grimsley, J. K.; Li, P.; Cerasoli, D. M.; Wild, J. R. *Protein Eng. Des. Sel.* **2008**, *21*, 405.
(55) Bashford, D. *Frontiers Sci.* **2004**, *9*, 1082.
(56) Nielsen, J. E.; McCammon, J. A. *Protein Sci.* **2003**, *12*, 313.
(57) Gomes, D. E.; Lins, R. D.; Pascutti, P. G.; Lei, C.; Soares, T. A. *J. Phys. Chem. B* **2009**, *114*, 531.
(58) Hammes-Schiffer, S.; Benkovic, S. J. *Annu. Rev. Biochem.* **2006**, *75*, 519.
(59) Tzeng, S. R.; Kalodimos, C. G. *Curr. Opin. Struct. Biol.* **2011**, *21*, 62.
(60) Mittermaier, A.; Kay, L. E. *Science* **2006**, *312*, 224.
(61) Vendruscolo, M.; Dobson, C. M. *Science* **2006**, *313*, 1586.
(62) Bhabha, G.; Lee, J.; Ekiert, D. C.; Gam, J.; Wilson, I. A.; Dyson, H. J.; Benkovic, S. J.; Wright, P. E. *Science* **2010**, *332*, 234.
(63) Boehr, D. D.; McElheny, D.; Dyson, H. J.; Wright, P. E. *Proc. Natl. Acad. Sci. U.S.A.* **2010**, *107*, 1373.
(64) Wright, P. E.; Dyson, H. J. *Curr. Opin. Struct. Biol.* **2009**, *19*, 31.
(65) Boehr, D. D.; McElheny, D.; Dyson, H. J.; Wright, P. E. *Science* **2006**, *313*, 1638.
(66) Eisenmesser, E. Z.; Millet, O.; Labeikovsky, W.; Korzhnev, D. M.; Wolf-Watz, M.; Bosco, D. A.; Skalicky, J. J.; Kay, L. E.; Kern, D. *Nature* **2005**, *438*, 117.
(67) Daniel, R. M.; Dunn, R. V.; Finney, J. L.; Smith, J. C. *Annu. Rev. Biophys. Biomol. Struct.* **2003**, *32*, 69.
(68) Korzhnev, D. M.; Salvatella, X.; Vendruscolo, M.; Di Nardo, A. A.; Davidson, A. R.; Dobson, C. M.; Kay, L. E. *Nature* **2004**, *430*, 586.
(69) Boehr, D. D.; Nussinov, R.; Wright, P. E. *Nat. Chem. Biol.* **2009**, *5*, 789.
(70) Dumas, D. P.; Caldwell, S. R.; Wild, J. R.; Raushel, F. M. *J. Biol. Chem.* **1989**, *264*, 19659.